Inorg. Chem. **2005**, *44*, 989–995

$Cu(HCO_2)_2(pym)$ (pym = pyrimidine): Low-Dimensional Magnetic Behavior and Long-Range Ordering in a Quantum-Spin Lattice

J. L. Manson,*,†,‡ T. Lancaster,§ L. C. Chapon,|| S. J. Blundell,§ J. A. Schlueter,⊥ M. L. Brooks,§ F. L. Pratt,# C. L. Nygren,▽ and J. S. Qualls◆

Department of Chemistry and Biochemistry, Eastern Washington University, Cheney, Washington 99004, Condensed Matter Sciences Division, Oak Ridge National Laboratory, Oak Ridge, Tennessee 37831, Clarendon Laboratory, Department of Physics, Oxford University, Oxford, OX1 3PU, U.K., ISIS Department, Rutherford Appleton Laboratory, Chilton, Didcot, OX11 0QX, U.K., Materials Science Division, Argonne National Laboratory, Argonne, Illinois 60439, ISIS Muon Facility, Rutherford Appleton Laboratory, Chilton, Didcot, OX11 0QX, U.K., Department of Chemistry, University of Tennessee, Knoxville, Tennessee 37996, and Department of Physics and Geology, University of Texas-Pan American, Edinburg, Texas 78539

Received September 13, 2004

We synthesized and structurally and magnetically characterized the novel 3D coordination polymer $Cu(HCO_2)_2$(pym) (pym = pyrimidine). The compound crystallizes in the monoclinic space group $C2/c$ with $a = 14.4639(8)$ Å, $b = 7.7209(4)$ Å, $c = 8.5172(5)$ Å, $\beta = 126.076(2)°$, and $V = 768.76(7)$ Å^3. In the structure buckled layers of $Cu(HCO_2)_2$ are interconnected by pym ligands to afford 1D Cu–pym–Cu chains. Bulk magnetic susceptibility measurements show a broad maximum at 25 K that is indicative of short-range magnetic ordering. Between 12 and 300 K a least-squares fit of the $\chi(T)$ data to a mean-field-corrected antiferromagnetic chain model yielded excellent agreement for $g = 2.224(3)$, $J/k_B = -26.9(2)$ K, and $zJ'/k_B = -1.1(3)$ K. Below ~3 K a transition to long-range magnetic ordering is observed, as suggested by a sharp and sudden decrease in $\chi(T)$. This result is corroborated by muon spin relaxation measurements that show oscillations in the muon asymmetry below $T_N = 2.802(1)$ K and rapidly fluctuating moments above T_N.

Introduction

Small, multidentate anions such as CN^-,[1] $[N(CN)_2]^-$,[2] $[C(CN)_3]^-$,[2] N_3^-,[3] and $C_2O_4^{2-}$[4] have been utilized in the design and synthesis of novel compounds that exhibit long-range magnetic ordering, some with T_c's that exceed room temperature.[1] The dimensionality of the structures can be tuned by virtue of the metal ion selected and whether other ligands such as chelates are present. The ability to predict structural and physical properties of new materials has been a major challenge welcomed by chemists working in the area of molecular magnetism.

Currently, the smallest carboxylate building block, i.e., formate ion, HCO_2^-, is being actively studied, and it has proven to be an effective bridging ligand and superexchange mediator in transition-metal-containing coordination polymers. In addition to the various hydrate forms that have been known for many years,[5] other examples that contain organic ligands have begun to emerge. Several dimeric complexes

* To whom correspondence should be addressed. E-mail: jmanson@ewu.edu.
† Eastern Washington University.
‡ Oak Ridge National Laboratory.
§ Oxford University.
|| ISIS Department, Rutherford Appleton Laboratory.
⊥ Argonne National Laboratory.
ISIS Muon Facility, Rutherford Appleton Laboratory.
▽ University of Tennessee.
◆ University of Texas-Pan American.

(1) (a) Hatlevik, O.; Buschmann, W. E.; Zhang, J.; Manson, J. L.; Miller, J. S. *Adv. Mater.* **1999**, *11*, 914. (b) Holmes, S. M.; Girolami, G. S. *J. Am. Chem. Soc.* **1999**, *121*, 5593. (c) Verdaguer, M.; Bleuzen, A.; Marvaud, V.; Vaissermann, J.; Seuleiman, M.; Desplanches, C.; Scuiller, A.; Train, C.; Garde, R.; Gelly, G.; Lomenech, C.; Rosenman, I.; Veillet, P.; Cartier, C.; Villain, F. *Coord. Chem. Rev.* **1999**, *192*, 1023.

(2) Reviews: (a) Miller, J. S.; Manson, J. L. *Acc. Chem. Res.* **2001**, *34*, 563 and references therein. (b) Batten, S. R.; Murray, K. S. *Coord. Chem. Rev.* **2003**, *246*, 103 and references therein.

(3) See, for example: (a) Ray, U.; Jasimuddin, S.; Ghosh, B. K.; Monfort, M.; Ribas, J.; Mostafa, G.; Lu, T. H.; Sinha, C. *Eur. J. Inorg. Chem.* **2004**, 250. (b) Fu, A. H.; Huang, X. Y.; Li, J.; Yuen, T.; Lin, C. L. *Chem. Eur. J.* **2002**, *8*, 2239.

(4) See, for example: Decurtins, S.; Pellaux, R.; Antorrena, G.; Palacio, F. *Coord. Chem. Rev.* **1999**, *192*, 841.

10.1021/ic048723x CCC: $30.25
Published on Web 01/15/2005

Scheme 1. Three Diazine Ligands Showing Possible Bidentate Coordination Modes

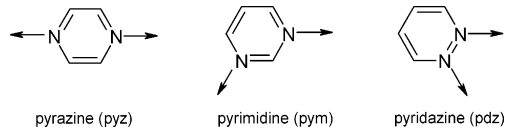

such as $Cu_2(HCO_2)_4L_2$ [L = urea,[6] dioxane,[7] dimethyl sulfoxide (DMSO),[7] and *N*,*N*-dimethylformamide (DMF)[8]] and the 1D chain compound $Cu(HCO_2)_2(py)_2 \cdot H_2O$[9] (py = pyridine) have been reported. The majority of reported structures though are inherently two-dimensional and include the aforementioned hydrates, $Co(HCO_2)_2(DMF)_2$[10] and $M(HCO_2)_2(urea)_2$ (M = Mn, Fe, Co, Ni, Cd, Zn).[11] Three-dimensional structures have been relatively unknown until recently and include $Cu(HCO_2)_2(pyz)$ (pyz = pyrazine),[12] $Cu(HCO_2)_2(4,4'\text{-bipy})$ (bipy = bipyridine),[12] $Mn_3(HCO_2)_6$,[13] $Mn(HCO_2)_3$,[14] and [AmineH][$Mn(HCO_2)_3$].[15]

In continuing our work on formate-based coordination polymers we extended our studies to include other diazine ligands such as pyrimidine (pym or 1,3-diazine). The corrugated 2D $Cu(HCO_2)_2$ layer found in $Cu(HCO_2)_2(pyz)$ offers the potential to accommodate a variety of molecules, thus producing an array of 3D lattice types. Specifically, the intralayer buckling affords an opposing 120° tilt of the CuO_4X_2 (X is a vacant axial position) chromophores, which allows successive layers to tightly pack together. Pyrimidine was chosen because the lone pairs on the sp^2 nitrogen atoms form a nominal 120° coordination angle (Scheme 1) that could lead to a network similar to $Cu(HCO_2)_2(pyz)$. From Scheme 1 it can be seen that the sp^2 nitrogen atoms in the other diazines, i.e., pyz and pyridazine (pdz), are arranged 180° and 60° apart, respectively, which profoundly affects the metal spacing, orbital orientations, and subsequent magnetic properties. By reacting $Cu(HCO_2)_2$ with pym, the anticipated $Cu(HCO_2)_2(pym)$ compound was formed which shows long-range magnetic ordering at low temperatures.

Table 1. X-ray Crystallographic Data for $Cu(HCO_2)_2(pym)$ Collected at 295 K

formula	$CuO_4N_2C_6H_6$
formula weight	233.67
space group	*C*2/*c*
a, Å	14.4639(8)
b, Å	7.7209(4)
c, Å	8.5172(5)
β, deg	126.076(2)
V, Å^3	768.76(7)
Z	4
ρ_{calc}, g/cm^3	2.019
λ, Å	0.71073
μ, mm^{-1}	2.821
$R^a(F)$	0.0297
$R_w{}^b(F)$	0.0799
GOF	0.870

^{a} $R = \sum[|F_o| - |F_c|]/\sum|F_o|$. ^{b} $R_w = [\sum w[|F_o| - |F_c|]^2/\sum w[|F_o|^2]^{1/2}$.

Table 2. Selected Bond Lengths (Å) and Bond Angles (deg) for $Cu(HCO_2)_2(pym)$ at 295 K

Cu−O(1)	2.398(1)	O(1)−Cu−O(2)	89.22(4)
Cu−O(2)	1.952(1)	N(1)−Cu−O(2)	89.31(5)
Cu−N(1)	2.060(1)	O(1)−Cu−N(1)	89.67(4)
C(1)−O(1)	1.238(2)	Cu−O(1)−C(1)	119.9(1)
C(1)−O(2)	1.250(2)	Cu−O(2)−C(1)	128.1(1)
N(1)−C(2)	1.337(2)	O(1)−C(1)−O(2)	125.7(1)
N(1)−C(4)	1.338(2)	N(1)−C(2)−C(3)	121.5(2)
C(2)−C(3)	1.381(2)	N(1)−C(4)−C(2)	117.5(1)

The structural and magnetic properties of $Cu(HCO_2)_2(pym)$ are described here and compared to $Cu(HCO_2)_2(pyz)$.

Experimental Section

Synthesis. In a typical synthesis a dilute aqueous solution of $Cu(HCO_2)_2 \cdot yH_2O$ (Aldrich, 0.500 g, 3.3 mmol) is mixed with pyrimidine (Acros, 0.261 g, 3.3 mmol) to afford a deep blue solution. X-ray-quality single crystals are obtained in 42% yield by slow evaporation of the solvent over a period of 1−2 weeks depending on the dilution used. Selected IR data (Nujol, cm^{-1}): 3115 w, 3093 w, 1600 s, 1562 s, 1411 m, 1335 s, 1086 m, 1038 w, 1010 w, 836 m, and 796 s.

X-ray Crystallography. A blue block measuring 0.45 × 0.20 × 0.20 mm^3 was mounted on a Bruker AXS SMART 1000 X-ray diffractometer equipped with a CCD area detector. Monochromated Mo Kα radiation (λ = 0.710 73 Å) was used in the data collection. Approximately a hemisphere of data was measured to a resolution of 0.75 Å at 295 K. The area detector frames were integrated by use of the program SAINT,[16] and the resulting intensities were corrected for absorption by Gaussian integration (SHELXTL program suite).[17] The SHELXTL program package was employed in the structure solution using direct methods and full-matrix least-squares refinement on F^2 (using all data). Positions of aromatic H atoms were calculated by employing a 'riding' model. All non-hydrogen atoms were refined with anisotropic thermal parameters. Additional details of the data collection are given in Table 1, while selected bond lengths and angles are listed in Table 2. Further details are available in the CIF deposited as electronic Supporting Information.

Magnetic Measurements. AC susceptibility measurements were conducted on a Lake Shore Cryotronics 7000 series susceptometer equipped with a low-temperature helium subpot option (allowing

(5) (a) Flippen, R. B.; Friedberg, S. A. *J. Chem. Phys.* **1963**, *38*, 2652. (b) Abe, H. *Phys. Rev.* **1953**, *92*, 1572. (c) Shimada, J.; Abe, H.; Ono, K. *J. Phys. Soc. Jpn.* **1956**, *11*, 137. (d) Wagner, G. R.; Friedberg, S. A. *Phys. Lett.* **1964**, *9*, 11.
(6) Uekusa, H.; Ohba, S.; Saito, Y. *Acta Crystallogr.* **1989**, *C45*, 377.
(7) Sapina, F.; Burgos, M.; Escriva, E.; Folgado, J.-V.; Beltran, D.; Gomez-Romero, P. *Inorg. Chim. Acta* **1994**, *216*, 185.
(8) Cejuda, R.; Alzuet, G.; Borras, J.; Liu-Gonzalez, M.; Sanz-Ruiz, F. *Polyhedron* **2002**, *21*, 1057.
(9) Cartwright, B. A.; Couchman, L.; Skapski, A. C. *Acta Crystallogr.* **1979**, *B35*, 824.
(10) Rettig, S. J.; Thompson, R. C.; Trotter, J.; Xia, S. *Inorg. Chem.* **1999**, *38*, 1360.
(11) See, for example: (a) Takeda, K.; Mito, M.; Nakajima, K.; Kakurai, K.; Yamagata, K. *Phys. Rev. B* **2001**, *63*, 024425. (b) Tokita, M.; Zenmyo, K.; Kubo, H.; Takeda, K.; Yamagata, K. *Physica B* **2000**, *284*, 1497. (c) Takeda, K.; Deguchi, H.; Hoshiko, T.; Yamagata, J. *J. Phys. Soc. Jpn.* **1989**, *58*, 3489.
(12) Manson, J. L.; Lecher, J. G.; Gu, J.; Geiser, U.; Schlueter, J. A.; Henning, R.; Wang, X.; Schultz, A. J.; Koo, H.-J.; Whangbo, M.-H. *J. Chem. Soc., Dalton Trans.* **2003**, 2905.
(13) Wang, Z.; Zhang, B.; Fujiwara, H.; Kobayashi, H.; Kurmoo, M. *Chem. Commun.* **2004**, 416.
(14) Cornia, A.; Caneschi, A.; Dapporto, P.; Fabretti, A. C.; Gatteschi, D.; Malavasi, W.; Sangregorio, C.; Sessoli, R. *Angew. Chem., Int. Ed.* **1999**, *38*, 1780.
(15) Wang, Z.; Zhang, B.; Otsuka, T.; Inoue, K.; Kobayashi, H.; Kurmoo, M. *J. Chem. Soc., Dalton Trans.* **2004**, 2209.
(16) Data Integration Software. *SAINT*, version 5.00; Bruker AXS, Inc.: Madison, WI, 1999.
(17) Structure Solution and Refinement Software. *SHELXTL*, version 5.0; Bruker AXS, Inc.: Madison, WI, 1996.

measurements to as low as 1.6 K to be achieved). A 1 Oe amplitude field oscillating at a frequency of 125 Hz was utilized for all measurements. A powder sample weighing ~187 mg was loaded into Delrin sample holders and affixed to the end of an aluminum rod. The samples were cooled from 300 to 4.5 K over a period of ~15 min and then further cooled to 1.5 K over a period of ~30 min. The real and imaginary components, χ' and χ'', respectively, of the volume AC susceptibility were recorded every 0.05 K.

For magnetization measurements a Quantum Design Physical Properties Measurement System (PPMS) ac/dc magnetometer equipped with a 9 T superconducting magnet and reciprocating sample option was used. Homogeneous powder samples were loaded into gelatin capsules and mounted on the end of a carbon fiber rod. For the broad temperature scan the sample was cooled in zero field to the lowest achievable temperature of 2 K, the magnet charged to 1 kOe, and data collected on warming to 300 K. Low-temperature zero-field-cooled $M(T)$ data were recorded for magnetic field strengths of 2, 3, 4, 5, 6, 7, 8, and 9 T. Isothermal $M(H)$ measurements were carried out at 1.3 K at the National High Magnetic Field Laboratory (Tallahassee, FL) in magnetic fields up to $\mu_0 H = 27$ T using a torque magnetometer. All magnetic data were corrected for core diamagnetism using Pascal's constants and temperature-independent paramagnetism (60×10^{-6} emu/mol for Cu^{2+} ion).

Muon Spin Relaxation. Zero-field muon spin relaxation (ZF μ^+SR) measurements have been made on a powder sample of Cu(HCO$_2$)$_2$(pym) using the MuSR instrument at the ISIS facility, Rutherford Appleton Laboratory, U.K., using a standard orange cryostat. The sample was wrapped in silver foil and mounted on a silver sample holder.

In a μ^+SR experiment[18] spin-polarized positive muons are stopped in a target sample, where the muon usually occupies an interstitial position in the crystal. The observed property in the experiment is the time evolution of the muon spin polarization, the behavior of which depends on the local magnetic field at the muon site. Each muon decays, with a lifetime of 2.2 μs, into two neutrinos and a positron, the latter particle being emitted preferentially along the instantaneous direction of the muon spin. Recording the time dependence of the positron emission directions therefore allows determination of the spin polarization of the ensemble of muons. In our experiments positrons are detected by detectors placed forward (F) and backward (B) of the initial muon polarization direction. Histograms $N_F(t)$ and $N_B(t)$ record the number of positrons detected in the two detectors as a function of time following the muon implantation. The quantity of interest is the decay positron asymmetry function which is defined as

$$A(t) = \frac{N_F(t) - \alpha N_B(t)}{N_F(t) + \alpha N_B(t)} \quad (1)$$

where α is an experimental calibration constant. $A(t)$ is proportional to the spin polarization of the muon ensemble.

Results and Discussion

Crystal Structure. Cu(HCO$_2$)$_2$(pym) crystallizes in the monoclinic space group $C2/c$ with four molecules per unit cell. The Cu^{2+} ion lies on an inversion center (Wyckoff position 4*c*), while C(3), H(3A), C(4), and H(4A) reside on the 2-fold axis (Wyckoff position 4*e*). All other atoms occupy general positions. Each Cu^{2+} ion is coordinated to four different formate oxygen atoms: two Cu−O(1) with bond distances of 2.398(1) Å are in axial positions, whereas two Cu−O(2) distances are 1.952(1) Å and occupy the equatorial plane along with two nitrogen atoms from the pym ligands [2× Cu−N(1) = 2.060(1) Å] (Figure 1). The Cu−O(1) bond length is similar to the Cu−O(2) distance found in Cu(HCO$_2$)$_2$(pyz) [2.371(2)Å], while Cu−O(2) is much longer in Cu(HCO$_2$)$_2$(4,4′-bipy) [2.528(2)Å].[12] Aside from the Jahn−Teller elongation along the O(1)−Cu−O(1A) axis, the CuO_4N_2 octahedron in Cu(HCO$_2$)$_2$(pym) is quite regular, the greatest deviation from 90° being 89.22(4)° for O(2)−Cu−O(1). The N(1)−Cu−N(1A), O(1)−Cu−O(1A), and O(2)−Cu−O(2A) bond angles are 180° as required by symmetry. Formate oxygen atoms coordinated to the Cu center, i.e., O(1) and O(2), form bond angles of 119.9(1)° and 128.1(1)° for Cu−O(1)−C(1) and Cu−O(2)−C(1), respectively. Comparing these bond angles to those of the pyz [120.5(2)° and 128.6(2)°] and 4,4′-bipy [117.2(2)° and 129.7(2)°] compounds reveals a clear similarity.[12] There is a larger difference, however, when we compare the Cu−O−C angles of 105.8(1)° and 133.5(2)° observed for the mixed-anion compound Cu(HCO$_2$)(NO$_3$)(pyz).[19] All bond lengths and angles for the HCO_2^- and pym ligands are in accord with those generally observed.[12]

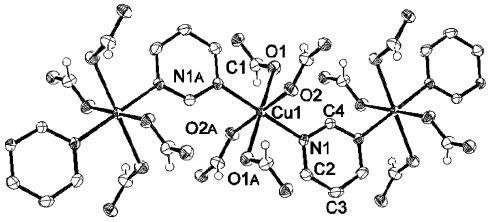

Figure 1. ORTEP diagram and atom-labeling scheme for Cu(HCO$_2$)$_2$(pym) showing the dominant Cu−pym−Cu superexchange pathway. pym hydrogen atoms have been omitted for clarity. Thermal ellipsoids are drawn at the 50% probability level.

Anti−anti formate anions join Cu^{2+} ions together to form corrugated 2D layers (Figure 2) within the *bc* plane, while neutral pym ligands join them together along the *a* direction to afford a noninterpenetrating 3D lattice (Figure 3). Each CuO_4N_2 octahedron is tilted with respect to neighboring octahedra, meaning that the Jahn−Teller axes are tilted accordingly. Cu···Cu separations along the Cu−pym−Cu and Cu−O−C(H)−O−Cu pathways are, respectively, 5.845 and 5.748 Å, which leads to voids apparently too small to accommodate interstitial solvent molecules.

When the structure of Cu(HCO$_2$)$_2$(pym) is viewed parallel to the *b* or *c* axes, its structure is indistinguishable from that of the pyz derivative. The only real difference between the two structures is the manner in which the Cu ions are linked by the diazine ligand, L, as shown in Scheme 2. In each case the Cu−L−Cu chains are linear with the Cu ions being equidistant. There are two types of chains in Cu(HCO$_2$)$_2$(pyz), one running parallel to (110) and the other propagating along (1−10), with all chains in the same "layer" being aligned along a common direction. The Cu−L−Cu chains

(18) Blundell, S. J. *Contemp. Phys.* **1999**, *40*, 175.

(19) Manson, J. L.; Lancaster, T.; Schlueter, J. A.; Nygren, C.; Blundell, S. J.; Brooks, M. L.; Pratt, F. L.; Koo, H.-J.; Whangbo, M.-H., manuscript in preparation.

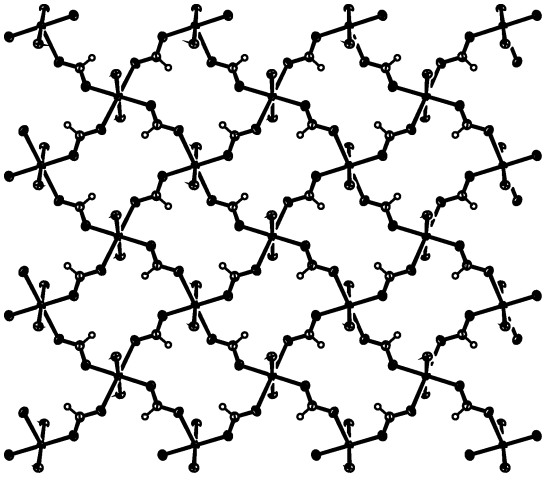

Figure 2. Portion of the corrugated 2D layers found in $Cu(HCO_2)_2(pym)$ showing the Cu−O−C(H)−O−Cu connectivity. Only the coordinated N atoms of the pym ligands are shown.

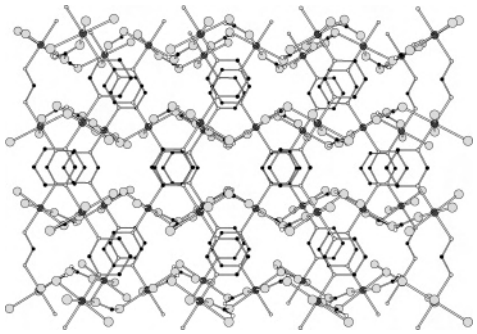

Figure 3. Three-dimensional framework of $Cu(HCO_2)_2(pym)$ viewed along the *c* axis. Pyrimidine hydrogen atoms have been omitted for clarity. Cu, O, N, and C atoms are depicted as heavily shaded, lightly shaded, open, and filled spheres, respectively.

Scheme 2. Schematic Comparing the Two Types of Linear Cu−L−Cu Chains Present in $Cu(HCO_2)_2L$ [L = pyz (a) and pym (b)][a]

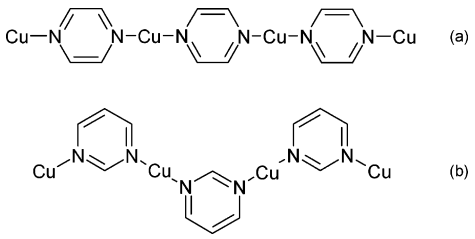

[a] Note that in both cases the Cu ions are uniformly spaced and lie along a common axis.

in $Cu(HCO_2)_2(pym)$ possess a single orientation that runs roughly perpendicular to the *bc* plane, i.e., approximately 36° away from the crystallographic *a* axis.

Short- and Long-Range Magnetic Ordering. Temperature Dependence. A plot of χT (Figure 4) shows a continuous decrease from a value of 0.424 emu K/mol at 300 K to 0.010 emu K/mol at 2 K. The value of χT at 300 K exceeds the value of 0.375 emu K/mol predicted for uncoupled $S = {}^1/_2$ ions; however, owing to *g*-value anisotropy this is not unexpected. The nature of the χT curve strongly suggests that all magnetic exchange interactions are antiferromagnetic. This finding was verified by a mean-field-corrected fit to a $S = {}^1/_2$ antiferromagnetic chain model with intrachain *J*, interchain exchange *J′*, with each chain having

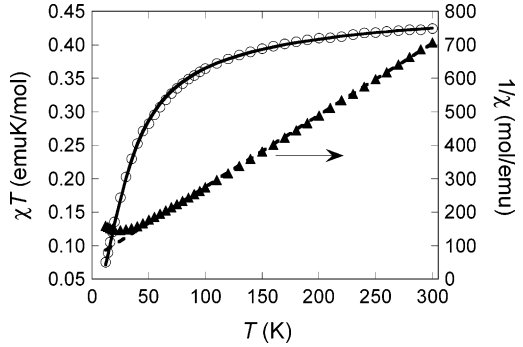

Figure 4. χT (○) and $1/\chi$ (▲) for $Cu(HCO_2)_2(pym)$ measured in a 1 kOe dc field. Solid and broken lines are theoretical fits to the Bonner−Fisher chain model and Curie−Weiss expression, respectively, as described in the text.

Table 3. Comparison of Exchange Coupling Constants and pym Coordination Modes in Some Cu^{2+} Complexes

compound	J/k_B (K)	pym bonding mode[a]	ref
$Cu(HCO_2)_2(pym)$	−26.9	eq−eq	this work
$Cu(dca)(NO_3)(pym)(H_2O)$[b]	−42.6	eq−eq	25a
$Cu_3(dca)_6(pym)_2$	−69.4	eq−eq	25a
$Cu(dca)_2(pym)\cdot CH_3CN$	>−1	ax−ax	31
$Cu(NO_3)_2(pym)(H_2O)_2$	−18	eq−eq	25d
$Cu(NO_3)_2(pym)_3$	+0.9	ax−eq	25d
$Cu(hfac)_2(pym)$[c]	+0.2	ax−eq	25b,c

[a] eq−eq = equatorial−equatorial, ax−eq = equatorial−axial, ax−ax = axial−axial. [b] dca = dicyanamide = $[N(CN)_2]^-$. [c] hfac = hexafluoroacetylacetonate.

z nearest neighbors.[20] A least-squares fit of χT to the model generated excellent agreement for the following parameters: $g = 2.224(3)$, $J = -26.9(2)$, and $zJ' = -1.1(3)$ K.[21] *J* and zJ' are assigned to the Cu−pym−Cu and Cu−O−C(H)−O−Cu exchange interactions, respectively. A fit of $1/\chi$ to a Curie−Weiss expression afforded $g = 2.229(3)$ and $\theta = -28.2(5)$ K, the negative θ value indicating the presence of antiferromagnetic correlations between Cu^{2+} sites (Figure 4). Furthermore, the fitted *J* value is in very good agreement with the absolute value of 26.6 K calculated from the expression $k_BT_{max}/J = 1.12S(S+1) + 0.10$ that relates the *J* value of a 1D magnetic system to the temperature, T_{max}, where $\chi(T)$ reaches a maximum.[22] Table 3 compares the *J* values and corresponding pym coordination modes observed in other polymeric materials.

Analogous to that found in $Cu(HCO_2)_2(pyz)$, there is an alternation of the magnetic Cu $d_{x^2-y^2}$ orbitals that occupy the equatorial CuN_2O_2 plane within the 2D $Cu(HCO_2)_2$ layers. The small zJ' value is then likely due to a competition between antiferromagnetic and ferromagnetic exchange interactions where the net coupling is slightly antiferromagnetic. This finding is in contrast to the large exchange coupling, i.e., $J/k_B = -73.2$ K, observed in $Cu(HCO_2)_2(H_2O)_4$ which leads to $T_N = 16.54$ K.[5a,23] In the tetrahydrate the magnetic $d_{x^2-y^2}$ orbitals exclusively occupy the 2D $Cu(HCO_2)_2$ layers, which affords very good orbital overlap.

(20) (a) Bonner, J. C.; Fisher, M. E. *Phys. Rev. A* **1964**, *135*, 640. (b) Ginsberg, A. P.; Lines, M. E. *Inorg. Chem.* **1972**, *11*, 2289.
(21) A least-squares fit of the $\chi(T)$ data to the same theoretical model as described in the text yielded parameters identical to those obtained for the $\chi T(T)$ analysis.
(22) Lines, M. E. *J. Phys. Chem. Solids* **1970**, *31*, 101.

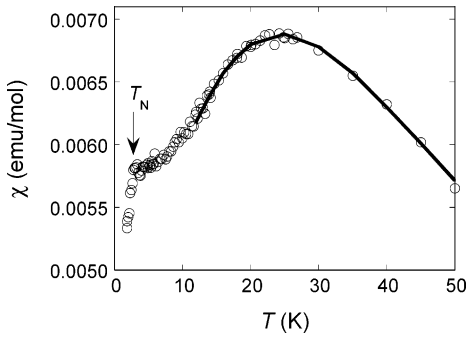

Figure 5. Low-temperature $\chi(T)$ plot of Cu(HCO$_2$)$_2$(pym) showing the broad maximum and abrupt decrease in $\chi(T)$ associated with the short- and long-range magnetic orderings. The solid line is the theoretical curve generated from the $\chi T(T)$ fit.

Upon cooling from 300 K, $\chi(T)$ increases gradually, reaching a value of 0.00685 emu/mol at 25 K where a broad maximum is observed. Below χ_{max}, $\chi(T)$ decreases smoothly until ~3 K, where it decreases abruptly (Figure 5). AC measurements indicate that these features do not depend on the frequency of the oscillating magnetic field. The origin of the broad maximum is likely due to short-range magnetic ordering within the Cu−pym−Cu chains, while the origin of the sharp decline in $\chi(T)$ is not completely clear but may be due to a structural or magnetic phase transition. The only other example that we aware of which shows a similar response in $\chi(T)$ is the spin-Peierls compound (TTF)Cu[S_4C_4-$(CF_3)_4$] (TTF = tetrathiafulvalene).[24]

It is known that μ-bridging pym can stabilize either antiferromagnetic or ferromagnetic exchange interactions depending on the magnetic orbital configuration of the transition metal to which it is attached. In the case of $S = {}^1/_2$ copper and vanadyl complexes, molecular orbital calculations suggest that equatorial−equatorial (eq−eq) and axial−axial (ax−ax) coordination favors orbital overlap, i.e., antiferromagnetic coupling, while a mixed axial−equatorial (ax−eq) situation leads to ferromagnetic interactions between Cu $d_{x^2-y^2}$ magnetic orbitals and nitrogen nσ and pπ orbitals of pym.[25] Thus, the antiferromagnetic coupling observed in Cu(HCO$_2$)$_2$(pym) can be understood in terms of its crystal structure, which shows eq−eq coordination of the pym ligand.

Field Dependence. The zero-field magnetization, $M(T)$, for Cu(HCO$_2$)$_2$(pym) was measured in various external fields between 2 and 9 T, and selected data are presented in Figure 6. In a 2 T field the magnetization shows a subtle downward inflection near 4 K, and as the field is increased, the data

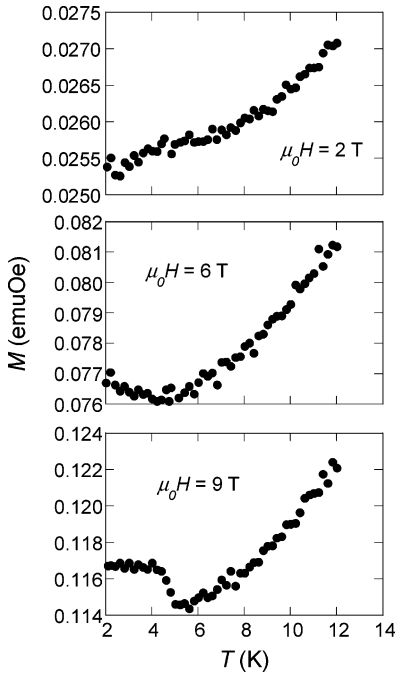

Figure 6. Zero-field-cooled $M(T)$ data for Cu(HCO$_2$)$_2$(pym) measured at 2, 6, and 9 T.

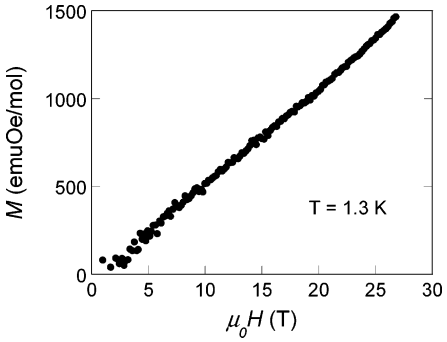

Figure 7. $M(H)$ plot for Cu(HCO$_2$)$_2$(pym) recorded at 1.3 K.

begin to curve upward for H approaching 8 T. At $\mu_0H = 9$ T the data take on a different appearance in that there is a sudden rise in $M(T)$ at 5 K which then levels off below 4 K. This behavior may be due to a spin flip transition; however, detailed measurements on single crystals are planned to help sort this out.

The isothermal magnetization, $M(H)$, was measured at 1.3 K up to 27 T and is shown in Figure 7. It can be seen that $M(H)$ initially rises slowly with an almost linear slope. Near 12 T the data curve upward and thus continue to rise up to the highest attainable field. This type of behavior has been observed in other low-dimensional $S = {}^1/_2$ quantum antiferromagnets.[26] At 27 T, M reaches a value of 1454 emu Oe/mol, which is ~77% below the predicted value of 6210 emu Oe/mol based on the fitted g value of 2.224. From the mean-field prediction of the zero-temperature saturation field, H_{sat}-(0), we can estimate the field necessary to overcome the antiferromagnetic interaction and fully align the Cu^{2+}

(23) (a) Kobayashi, H.; Haseda, T. *J. Phys. Soc. Jpn*. **1963**, *18*, 541. (b) Seehra, M. S. *Phys. Lett*. **1969**, *28A*, 754. (c) Koyama, K.; Nobumasa, H.; Matsuura, M. *J. Phys. Soc. Jpn*. **1987**, *56*, 1553.

(24) (a) Bray, J. W.; Hart, H. R.; Interrante, L. V.; Jacobs, I. S.; Kasper, J. S.; Watkins, G. D.; Wee, S. H.; Bonner, J. C. *Phys. Rev. Lett*. **1975**, *35*, 744. (b) Jacobs, I. S.; Bray, J. W.; Hart, H. R.; Interrante, L. V.; Kasper, J. S.; Watkins, G. D.; Prober, D. E.; Bonner, J. C. *Phys. Rev. B* **1976**, *14*, 3036.

(25) (a) Manson, J. L.; Gu, J.; Schlueter, J. A.; Wang, H.-H. *Inorg. Chem*. **2003**, *42*, 3950. (b) Ishida, T.; Nakayama, K.; Nakagawa, M.; Sato, W.; Ishikawa, Y.; Yasui, M.; Iwasaki, F.; Nogami, T. *Synth. Met*. **1997**, *85*, 1655. (c) Yasui, M.; Ishikawa, Y.; Ishida, T.; Nogami, T.; Iwasaki, F. *Acta Crystallogr*. **2001**, *B57*, 772. (d) Yasui, M.; Ishikawa, Y.; Akiyama, N.; Ishida, T.; Nogami, T.; Iwasaki, F. *Acta Crystallogr*. **2001**, *B57*, 288.

(26) See, for example: (a) Amaral, S.; Jensen, W. E.; Landee, C. P.; Turnbull, M. M.; Woodward, F. M. *Polyhedron* **2001**, *20*, 1317. (b) Bordallo, H. N.; Chapon, L.; Manson, J. L.; Ling, C. D.; Qualls, J. S.; Hall, D.; Argyriou, D. N. *Polyhedron* **2003**, *22*, 2045.

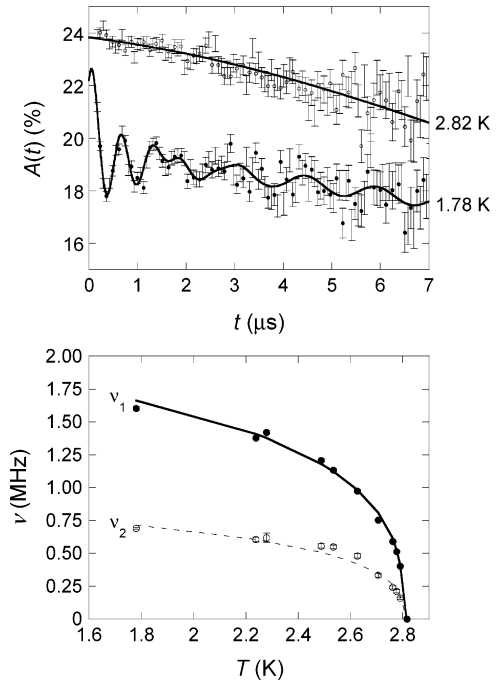

Figure 8. (a) ZF μ^+SR spectra measured at 1.78 and 2.82 K showing oscillations below the ordering temperature $T_N = 2.802(1)$ K. Data measured above T_N display a Gaussian form at high temperatures. (b) Temperature evolution of the two oscillation frequencies. The solid and dashed lines are fits to eq 4.

magnetic moments according to eq 2[26a]

$$\mu_0 H_{sat}(0) = 2zJ/(g\mu_B) \quad (2)$$

From this equation we derive $\mu_0 H_{sat}(0) = 48.4$ T for $z = 2$, $J/k_B = 26.9$ K, and $g = 2.224$. We note that since the Cu−pym−Cu "chains" in $Cu(HCO_2)_2(pym)$ are not completely isolated, the actual saturation field is likely higher than that estimated owing to additional interchain antiferromagnetic interactions. Hence, 48.4 T should be taken as the minimum saturation field.

Muon Spin Relaxation. We chose μ^+SR to further study the origin of the low-temperature anomaly because muons are especially sensitive to small magnetic moments. Figure 8a shows examples of ZF asymmetry spectra measured for this material. For temperatures $T \geq 2.82$ K, the observed asymmetry spectra show Gaussian relaxation, characteristic of the muon ensemble experiencing a static, random array of local magnetic fields. This field distribution is most likely due to the randomly oriented nuclear moments in the material, with the contribution from the fast-fluctuating electronic moments outside the muon time scale in this temperature regime. This hypothesis is consistent with our observation that an applied field of as little as 1 mT, directed parallel to the initial muon spin direction, repolarizes the muon ensemble [i.e., $\lim_{t\to\infty} A(t) = A(0)$], as expected for relaxation due to static, disordered field distribution.[27]

At temperatures $T < 2.82$ K oscillations in the positron asymmetry are clearly observable (Figure 8a). These oscillations are characteristic of a quasistatic local magnetic field at the muon site, which causes a coherent precession of the spins of those muons with a component of their spin polarization perpendicular to this local field. The frequencies of the oscillations (which are proportional to the order parameter in the broken symmetry phase) are given by $\nu_i = \gamma_\mu B_i/2\pi$, where γ_μ is the muon gyromagnetic ratio ($\equiv 2\pi \times 135$ MHz T^{-1}) and B_i is the local field at the ith muon site. The presence of oscillations in the muon asymmetry for $T < 2.82$ K provides strong evidence for the existence of long-range magnetic order (LRO) but not a spin-Peierls transition.

Two distinct precession frequencies are found in our data below T_N, suggesting the existence of two distinct muon stopping sites in $Cu(HCO_2)_2(pym)$. We note that two precession frequencies have been observed in muon studies of related materials.[19,28,29] To extract the temperature dependence of these frequencies, the spectra for $T < 2.82$ K were successfully fitted to a function of the form

$$A(t) = A_1 \exp(-\lambda_1 t)\cos(2\pi\nu_1 t + \phi_1) + A_2 \exp(-\lambda_2 t)\cos(2\pi\nu_2 t + \phi_2) + A_3 \exp(-\lambda_3 t) \quad (3)$$

where $\phi_{1,2}$ are phases and $\lambda_{1,2}$ are temperature-dependent relaxation rates. The parameters A_3 and λ_3 reflect a temperature-independent contribution to the signal from the component of the muon-spin polarization parallel to the local magnetic field and also from those muons which stop in the sample holder or cryostat tail.

The ratio of the contributions from the oscillating signals A_1:A_2 was found to be approximately 6:1, suggesting that the site associated with the frequency ν_1 is six times as probable as that associated with ν_2. The origin of the phase offsets ϕ_1 (=−39°) and ϕ_2 (=−31°) are unclear, although we note that similar phase offsets have also been observed in muon studies of related materials.[28] The magnitudes of the relaxation rates λ_i (which scale roughly with the frequencies ν_i) do not vary strongly with temperature but show a tendency to decrease as the magnetic phase transition is approached from below. This suggests that the spin relaxation is dominated by the magnitude of the local field at the muon site rather than the slowing of critical fluctuations.

The temperature dependence of the extracted precession frequencies is shown in Figure 8b. The lines shown are fits to the functional form

$$\nu_i(T) = \nu_i(0)\left[1 - \left(\frac{T}{T_N}\right)^{\delta}\right]^{\beta} \quad (4)$$

The paucity of data at low temperatures makes a reliable determination of the parameters in eq 4 problematic. If we make the assumption that $\delta = 2$, as would be expected for antiferromagnetic spin waves, we obtain $\nu_1(0) = 1.97(2)$ MHz (corresponding to a local field at the muon site of $B_1 = 14.5(1)$ mT), $\nu_2(0) = 0.844(1)$ MHz (or $B_2 = 6.23(1)$ mT),

(27) Hayano, R. S.; Uemura, Y. J.; Imazato, J.; Nishida, N.; Yamazaki, T.; Kubo, R. *Phys. Rev. B* **1979**, *20*, 850.

(28) Lancaster, T.; Blundell, S. J.; Pratt, F. L.; Brooks, M. L.; Manson, J. L.; Brechin, E. K.; Cadiou, C.; Low, D.; McInnes, E. J. L.; Winpenny, R. E. P. *J. Phys.: Condens. Matter* **2004**, *16*, S4563.

(29) Manson, J. L.; Lancaster, T.; Qiu, Y.; Kenzelmann, M.; Blundell, S. J.; Brooks, M. L.; Pratt, F. L., manuscript in preparation.

$\beta = 0.33(1)$, and $T_N = 2.802(1)$ K. We note that the value of β is similar to that observed for $(C_2H_5NH_3)_2CuCl_4$ ($\beta = 0.32$), which is comparable to that calculated for a 3D Ising system ($\beta = 0.312$).[30]

Conclusions

$Cu(HCO_2)_2(pym)$ is a novel quasi-1D antiferromagnet that exhibits a transition to long-range ordering below $T_N = 2.8$ K as shown by magnetic susceptibility and muon spin relaxation measurements. The HCO_2^- anions adopt an anti−anti bridging mode between the $S = {}^1/_2$ Cu^{2+} ions which affords a weak antiferromagnetic coupling relative to the interaction along Cu−pym−Cu, which is much stronger ($J/k_B = -26.9$ K). The present work also clearly demonstrated the need for additional techniques to determine the nature of anomalous magnetic behavior, in this case μ^+SR. Future studies on $Cu(HCO_2)_2(pym)$ will involve use of neutron scattering to study spin excitations in the absence and presence of external magnetic fields.

Acknowledgment. Oak Ridge National Laboratory is managed by UT-Battelle, LLC, for the U.S. Department of Energy under contract no. DE-AC05-00OR22725. Work at Argonne National Laboratory is supported by the Office of Basic Energy Sciences, Division of Materials Science, U.S. Department of Energy, under Contract W-31-109-ENG-38. J.L.M. acknowledges R. Feyerherm (HMI) for helpful discussions. We are grateful to J. Lord and P. King at the ISIS facility for technical assistance. This work is supported by the EPSRC.

Supporting Information Available: Crystallographic data in CIF format. This material is available free of charge via the Internet at http://pubs.acs.org.

IC048723X

(30) de Jongh, L. J.; Miedema, A. R. *Adv. Phys*. **1974**, *23*, 1.
(31) Riggio, I.; van Albada, G. A.; Ellis, D. D.; Spek, A. L.; Reedijk, J. *Inorg. Chim Acta* **2001**, *313*, 120.